ARTICLE

Air-Stable Electron Depletion of Bi_2Se_3 Using Molybdenum Trioxide into the Topological Regime

Mark T. Edmonds,[†,#] Jack T. Hellerstedt,[†,‡,#] Anton Tadich,[§] Alex Schenk,[⊥] Kane Michael O'Donnell,[§] Jacob Tosado,[†,‡] Nicholas P. Butch,[‡,∥] Paul Syers,[‡] Johnpierre Paglione,[‡] and Michael S. Fuhrer[†,‡,*]

[†]School of Physics, Monash University, Clayton, VIC 3800, Australia, [‡]Center for Nanophysics and Advanced Materials, University of Maryland, College Park, Maryland 20742-4111, United States, [§]Australian Synchrotron, Clayton, VIC 3168, Australia, [⊥]Department of Physics, La Trobe University, Bundoora, VIC 3086, Australia, and [∥]National Institute of Standards and Technology, Gaithersburg, Maryland 20899, United States. [#]These authors contributed equally to the paper.

ABSTRACT We perform high-resolution photoelectron spectroscopy on *in situ* cleaved topological insulator Bi_2Se_3 single crystals and *in situ* transport measurements on Bi_2Se_3 films grown by molecular beam epitaxy. We demonstrate efficient electron depletion of Bi_2Se_3 *via* vacuum deposition of molecular MoO_3, lowering the surface Fermi energy to within ∼100 meV of the Dirac point, well into the topological regime. A 100 nm MoO_3 film provides an air-stable doping and passivation layer.

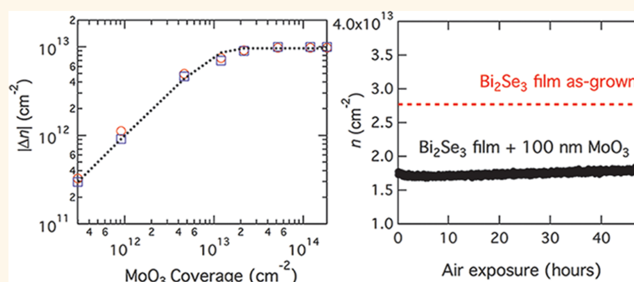

KEYWORDS: Bi_2Se_3 · topological insulator · molecular doping · air-stable capping layer

Topological insulators, such as Bi_2Se_3, are a new class of material that possesses topologically protected Dirac surface states that hold great promise for future nanoelectronic devices including spin generation and detection without ferromagnetism and dissipationless electronic transport in the quantum anomalous Hall state.[1−3] However, major challenges exist in realizing Bi_2Se_3 devices that operate in the topological regime in air. The first is that as-prepared Bi_2Se_3 is invariably n-type-doped due to selenium vacancies,[4] such that the Fermi level resides in the bulk conduction band, not within the Dirac surface states necessary to realize these electronic devices. The second is that Bi_2Se_3 when exposed to atmosphere becomes further n-type-doped and degrades over time.[5] This has led to significant work to tune the Fermi level into the bulk gap with approaches such as bulk substitutional doping or the electric field effect. Small concentrations of doping elements such as Ca are able to significantly reduce the density of electrons[6,7] but are not stable in ambient conditions, and large enough amounts of elements such as Pb and Sn are unable to be incorporated into the Bi_2Se_3 lattice to make it p-type.[8] Partial substitution of Sb for Bi has been a successful approach in obtaining low-doped samples; however, the substitutional disorder degrades the carrier mobility.[9] Tuning the Fermi level into the topological regime with the field effect also presents significant challenges, necessitating modulating charge densities often well in excess of 10^{13} cm^{-2}, difficult due to the large electric field required which is above the breakdown field of most conventional oxides.[10,11]

Surface transfer doping is another potential method to remove the n-type doping. It provides an alternative route to conventional bulk doping, as it does not involve introducing impurities into the bulk lattice and has been successfully implemented across a range of other materials.[12−15] In the case of acceptor doping, high electron affinity molecules deposited onto the surface result in the transfer of electrons from the substrate into the molecular overlayer. This form of molecular doping on Bi_2Se_3 was recently demonstrated using the strong electron-accepting molecule tetrafluoro-tetracyanoquinodimethane (F4-TCNQ) on

* Address correspondence to michael.fuhrer@monash.edu.

Received for review April 6, 2014 and accepted May 30, 2014.

Published online June 09, 2014
10.1021/nn502031k

© 2014 American Chemical Society

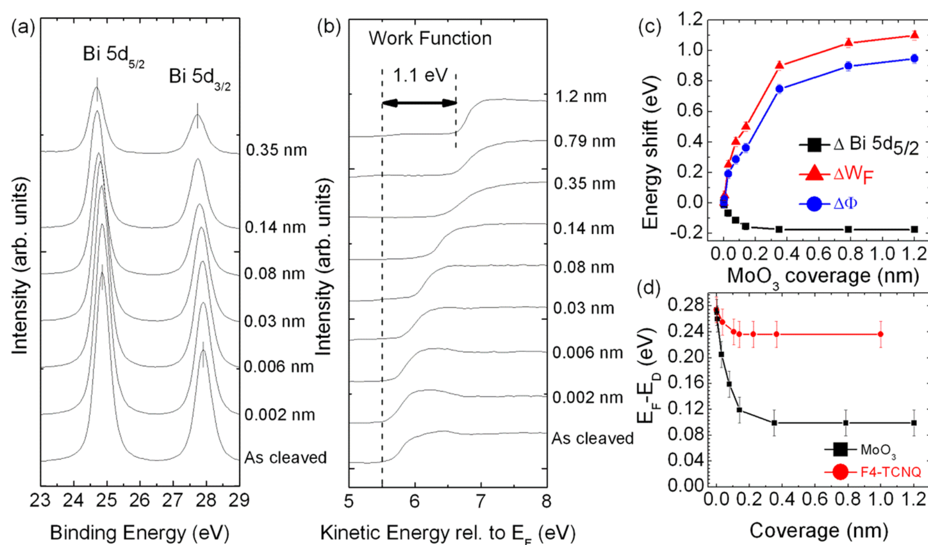

Figure 1. Molecular coverage-dependent Fermi energy and surface dipole. (a) Bismuth 5d core level spectra taken at $h\nu$ = 100 eV at selected MoO_3 coverages. (b) Secondary electron cutoff as a function MoO_3 coverage. (c) Energy level shifts for the Bi $5d_{5/2}$ core level (black squares), work function (red triangles), and interface dipole (blue circles) as a function of MoO_3 coverage [note: error bars smaller than plot symbol]. (d) $E_F - E_D$ plotted as a function of MoO_3 coverage (black squares) and F4-TCNQ coverage (red circles).

mechanically exfoliated thin Bi_2Se_3 crystals on SiO_2/Si substrates. It was found that enough excess charge was removed to place the Fermi level near the conduction band edge, allowing the field effect to be utilized to further tune the Fermi level through the topological regime.[16−18] Yet little is known about the mechanisms and limits of surface transfer doping on Bi_2Se_3, particularly the limits of effectiveness of doping, and whether other candidate molecules exist that can dope Bi_2Se_3 into the topological regime and remain stable after prolonged exposure to air.

Here we report high-resolution photoemission spectroscopy of lightly doped Bi_2Se_3 crystals (surface Fermi energy relative to Dirac point $E_F - E_D \sim 270$ meV) cleaved in vacuum and exposed to the molecular dopant MoO_3. Coverage-dependent photoemission spectroscopy of Bi core levels allows tracking of the Fermi energy shift, while Mo spectroscopy reveals the fraction of charged MoO_3 molecules and low-energy cutoff spectroscopy measures the work function. We find efficient acceptor doping by MoO_3, saturating at $E_F - E_D = 100$ meV, well within the topological regime. We observe an induced interface dipole of 0.74 eV, corresponding to $\sim 10^{13}$ cm^{-2} electrons transferred from the Bi_2Se_3. We implement a doping model based on Fermi–Dirac statistics to accurately describe the doping behavior including saturation. Furthermore, we demonstrate that a thick 100 nm passivation layer of MoO_3 can be used to deplete excess electrons from a Bi_2Se_3 thin film as well as prevent degradation of Bi_2Se_3 when it is exposed to atmosphere with the carrier density remaining nearly unchanged after 2 days of exposure.

RESULTS AND DISCUSSION

In Figure 1, the response of the Fermi level shift and work function of *in situ* cleaved Bi_2Se_3 samples to deposition of MoO_3 are measured using high-resolution surface-sensitive photoemission spectroscopy. Figure 1a plots the evolution of the bismuth 5d core level (at photon energy $h\nu$ = 100 eV) with increasing MoO_3 coverage. Both the Bi $5d_{5/2}$ and Bi $5d_{3/2}$ peak positions shift to lower binding energy (*i.e.*, the Fermi energy moves toward the Dirac point) with increasing coverage and reach saturated positions at a coverage of 0.34 nm. In Figure 1b, the secondary electron cutoff is plotted as a function of MoO_3 coverage. The work function of the freshly cleaved sample is 5.40 ± 0.03 eV and increases by up to 1.1 eV as the MoO_3 coverage increases. The saturated value of 6.5 eV at a coverage of 0.8 nm is in reasonable agreement with values reported for solid MoO_3,[19] indicating that the low-energy cutoff spectra are no longer probing the Bi_2Se_3−MoO_3 interface but only the MoO_3 overlayer. In Figure 1c, the change in Bi $5d_{5/2}$ peak position (black squares), the change in work function, ΔW_F (red triangles), and the interface dipole, $\Delta\Phi$ (blue circles), that forms as a result of the surface transfer doping process are plotted as a function of MoO_3 coverage. The binding energy of the Bi core level decreases by 0.18 ± 0.02 eV, consistent with the removal of electrons from the Bi_2Se_3. The work function increases by 1.1 eV, indicating the formation of a positive surface dipole that arises due to charge transfer across the Bi_2Se_3−MoO_3 interface. The interface dipole is given by $\Delta\Phi = \Delta W_F - \Delta(E_F - E_D)$, where $E_F - E_D$ is the position of the Fermi level relative to the Dirac point at each coverage plotted in Figure 1d (black squares). However, the work function value used to determine the interface dipole is only valid at low coverages (*i.e.*, up until charge transfer saturation), above which it starts to represent the measurement of the molecular overlayer, thus resulting in incorrect

determination of the doping-induced dipole. At 0.34 nm of MoO_3, an interface dipole of 0.73 ± 0.02 eV has built up at the Bi_2Se_3–MoO_3 interface. In Figure 1d, we plot $E_F - E_D$ for both MoO_3 (black squares) and F4-TCNQ (red circles) as a function of respective molecular coverage. In both cases, the as-cleaved samples have $E_F - E_D = 0.27 \pm 0.05$ eV (*i.e.*, the Fermi level lies 0.27 eV above the Dirac point energy). However, the response of $E_F - E_D$ to the two molecules is very different, with only a shift of 40 meV observed for F4-TCNQ, consistent with previous reports of doping to near the conduction band edge.[18] In contrast, for increasing MoO_3 coverage, the Fermi level moves toward the Dirac point, reaching a saturated value of 100 ± 20 meV above the Dirac point, placing the Fermi level well within the gap and in the topological regime. As discussed in more detail below, we believe the difference arises due to the significantly larger electron affinity of MoO_3 compared to F4-TCNQ, with values as high as 6.7 eV reported for thick MoO_3 films[19] compared to 5.24 eV for F4-TCNQ.[20] The measured work function of as-cleaved Bi_2Se_3 is 5.4 eV, placing the lowest unoccupied molecular orbital (LUMO) of F4-TCNQ above the Fermi level of the Bi_2Se_3 when the vacuum levels are aligned, meaning only a small amount of charge transfer is possible. In contrast, the larger electron affinity of MoO_3 places the LUMO position well below the Fermi level, allowing for charge transfer to take place.

We now discuss the Mo 3d photoemission spectra of the MoO_3 molecules in Figure 2a. We observe three distinct features: peaks at binding energies of 231.5 and 234.7 eV correspond to the Mo $3d_{5/2}$ and Mo $3d_{3/2}$ states, respectively. A third small peak at 228.3 eV is assigned to the 2s core level of sulfur, which we find associated with these Bi_2Se_3 samples. This was confirmed by taking angular-dependent spectra on as-cleaved samples and observing no change in intensity of the S 2s peak. This small amount of sulfur is incidental and plays no part in the following discussion. Remarkably, we observe that both the Mo $3d_{5/2}$ and Mo $3d_{3/2}$ features consist of two distinct peaks clearly separated in binding energy by ~0.8 eV and whose relative intensities (branching ratios) are the same for both $3d_{5/2}$ and $3d_{3/2}$. In Figure 2b, the Mo 3d spectrum taken at 0.14 nm coverage is plotted showing the peak fit with the two distinct components necessary to fit each peak. The observation is strong evidence for two chemically different states of the MoO_3 molecules on the surface of Bi_2Se_3. These we interpret as neutral (N_A) and ionized (N_A^-) MoO_3 acceptors. We can rule out the possibility of two species formed during evaporation of MoO_3 (*e.g.*, stoichiometric MoO_3 and MoO_3 with oxygen vacancies) as the relative intensities of the two components are strongly dependent on coverage. A similar effect was observed for surface transfer doping hydrogen-terminated diamond with

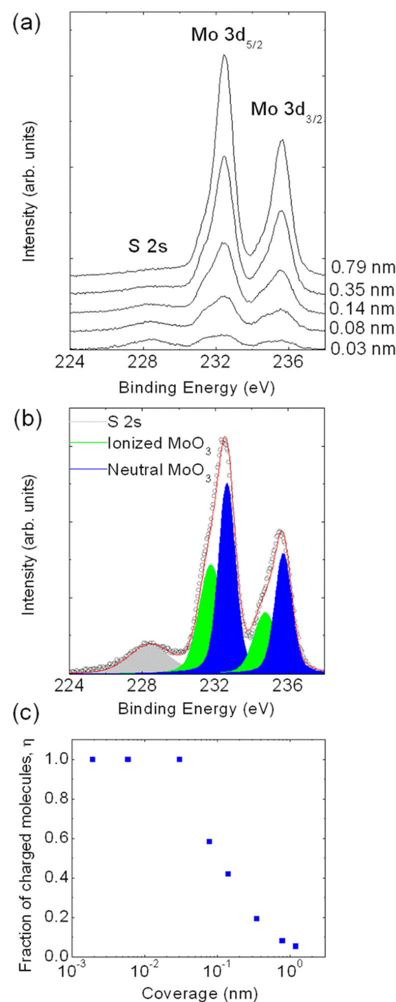

Figure 2. Measurement of the fraction of charged molecules using molybdenum core level spectroscopy. (a) Mo 3d core level spectra at selected MoO_3 coverages. (b) MoO_3 core level spectra at a coverage of 0.14 nm with peak fits illustrating the two clear MoO_3 charge states. (c) Relative fraction of ionized MoO_3 as a function of coverage of the two components: doping (N_A^-) and nondoping (N_A) that make up the Mo 3d core level of MoO_3 on Bi_2Se_3.

the fluorofullerene $C_{60}F_{48}$ where the two species correspond to neutral and singly ionized $C_{60}F_{48}$.[21] We identify the Mo 3d lines at lower binding energy with ionized molecules as the extra charge within a MoO_3 molecule is expected to lower all binding energies due to additional Coulomb repulsion.

The observation of neutral and charged MoO_3 in the photoemission spectra allows us to directly probe the fractional concentration $\eta = N_A^- / (N_A + N_A^-)$ of ionized molecules, where N_A^- and N_A are the relative peak areas at each coverage. Figure 2c shows η plotted as a function of coverage. As expected, at low coverage, η is near unity as all the molecules are ionized. At higher coverages, η drops as the induced surface dipole retards further charge transfer, and we observe a transition between mainly ionized MoO_3 below 0.14 nm to an increasing contribution of nondoping neutral MoO_3 for higher coverages until the charge

transfer process ceases at 0.35 nm. Beyond this coverage, additional MoO_3 remains neutral on the Bi_2Se_3 surface.

We are now in a position to understand the Fermi energy shift (Figure 1d) in terms of the amount of charge removed from the surface, as determined by the concentration of ionized MoO_3 (Figure 2c). In Figure 3a, we plot the charged MoO_3 molecules, N_A^-, expressed in monolayers (1 ML corresponds to a thickness of 0.65 nm[22]) as a function of $E_F - E_D$. We equate N_A^- with the change in charge density in the Bi_2Se_3 because we expect that only one electron is transferred per MoO_3 molecule, consistent with the observation of only two types of Mo core level spectra, and the expectation that strong intermolecular Coulomb interaction should yield positive effective correlation energy. In this case, and utilizing the linear dispersion of the 2D surface states, we can write down an equation describing the behavior of N_A^- with respect to $E_F - E_D$:

$$N_A^- = \frac{n_0}{\rho} - \frac{|E_F - E_D|^2}{\rho\pi(2\hbar v_F)^2} \qquad (1)$$

where ρ is the areal density of a monolayer of MoO_3 molecules per cm^2, n_0 is the initial sheet carrier density of the Bi_2Se_3 surface, and v_F is the Fermi velocity of electrons in Bi_2Se_3. [Note that we expect some additional contribution from bulk states in eq 1; however, the low Fermi energy of our as-cleaved crystals $E_F - E_D = 270$ meV is near the bulk band edge, so the surface state is expected to dominate the density of states.] The dashed line in Figure 3a is a fit to eq 1. The fit does not determine both ρ and v_F; however, assuming a Fermi velocity of $v_F = 3.5 \times 10^5$ ms^{-1} (refs 23 and 24) yields a value for the areal density for 1 ML of $\rho = 1.0 \times 10^{14}$ MoO_3 molecules cm^{-2}, in reasonable agreement with what would be expected from close-packing arguments based on the size of the MoO_3 molecule. Using $v_F = 3.5 \times 10^5$ ms^{-1} and the linear band dispersion, the as-cleaved samples ($E_F - E_D = 0.270$ eV) have an initial surface carrier density of $n_0 = 1.13 \times 10^{13}$ cm^{-2}. Upon saturation of the charge transfer process at a coverage of 0.34 nm of MoO_3 and $E_F - E_D = 0.10$ eV, the density is now $n = 1.47 \times 10^{12}$ cm^{-2}. Thus, almost $\sim 10^{13}$ cm^{-2} of electrons can be removed from the Bi_2Se_3 when MoO_3 is deposited onto the surface.

We can also compare the change in charge density $|\Delta n| = |n - n_0|$ as a function of the interface dipole, $\Delta\Phi$. Value of Δn is extracted from the experimentally measured $E_F - E_D$ values (red circles) using $v_F = 3.5 \times 10^5$ ms^{-1}, as well as independently from the number of ionized MoO_3 molecules (blue squares) using the areal density, $\rho = 1.0 \times 10^{14}$ obtained from Figure 3a. The result is shown in Figure 3b. In both cases, Δn is proportional to $\Delta\Phi$, with the same constant of proportionality, consistent with a simple electrostatic (capacitive) interpretation where $\Delta n = (C/e)\Delta\Phi$ and C is the capacitance per area associated with the separation of charge across a charge-free region at the Bi_2Se_3–MoO_3 interface. A linear fit of the data yields $C = 4.16$ μF cm^{-2} for the interface capacitance.

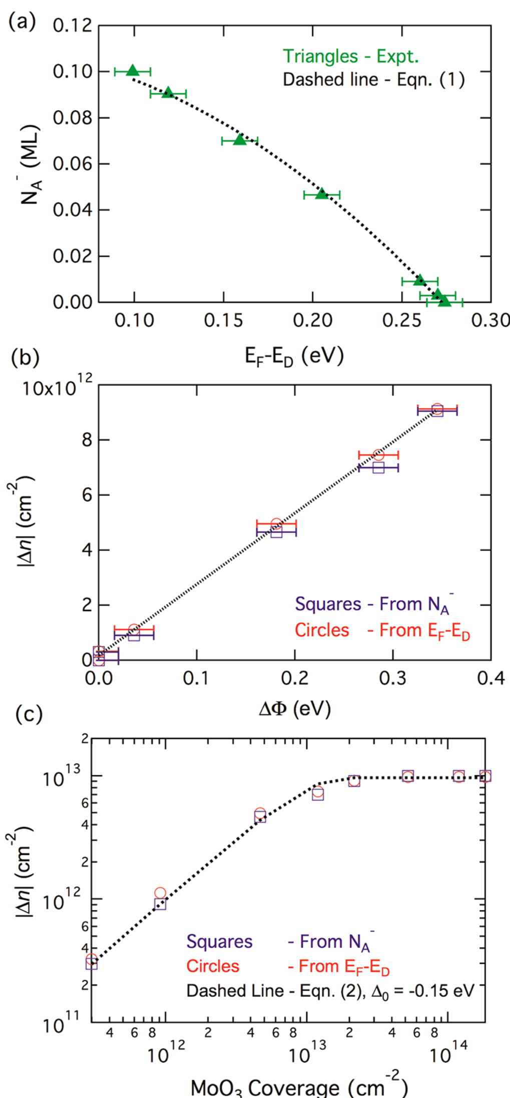

Figure 3. Comparison of experimental data and charge transfer model. (a) Number of charged MoO_3 molecules (monolayer, ML) plotted as a function of $E_F - E_D$. The black dashed line is a fit of the data using eq 1. (b) Change in carrier density $|\Delta n|$ as a function of interface dipole $\Delta\Phi$. (c) Change in carrier density $|\Delta n|$ as a function of MoO_3 coverage. In (b,c), blue squares show $|\Delta n|$ determined from the number of charged MoO_3 molecules (data in Figure 2c), and red circles show $|\Delta n|$ calculated from $E_F - E_D$ assuming a linear surface state dispersion. In (c), the black dashed line corresponds to the change in density calculated using eq 2 with initial activation energy of −0.15 eV.

It is important to understand the mechanism for charge transfer between the Bi_2Se_3 and MoO_3 overlayer. It has been shown that the charge transfer process from a substrate to a molecular overlayer is governed by Fermi–Dirac statistics applied to the molecular level into which the electron is transferred,[21,25] in this case, the lowest unoccupied molecular orbital of MoO_3. With all energies referenced to the

vacuum level, the LUMO energy corresponds to the electron affinity, χ_{MoO_3} of neutral MoO_3 in contact with the Bi_2Se_3. Then the doping fraction η can be expressed as

$$\eta = \frac{N_A^-}{N_A + N_A^-} = \frac{1}{\frac{1}{g}\exp[(\Delta_0 + \Delta\Phi + (E_D - E_F))/k_BT] + 1} \quad (2)$$

Here g is the degeneracy factor of the MoO_3 LUMO. As above, we equate N_A^- with the change in electron density in Bi_2Se_3, and Δ_0 is the initial activation energy before charge transfer has taken place, given by $\Delta_0 = W_{F,Bi_2Se_3} + (E_F - E_D) - \chi_{MoO_3}$, where W_{F,Bi_2Se_3} is the work function of Bi_2Se_3. Equation 2 allows us to determine the value of Δ_0 from the coverage dependence of η or Δn.

Figure 3c plots the experimentally determined $|\Delta n|$ as a function of MoO_3 coverage. The red circles represent the change in density determined using the values of $E_F - E_D$ in Figure 1d and eq 1. The blue squares are derived making use of the relative intensities of the MoO_3 core level components to determine the number of charged MoO_3 molecules at each coverage (Figure 2c). Overall, the agreement between these two independently derived values is very good. The dashed line in Figure 3c corresponds to the change in density calculated using eq 2 with initial acceptor energy of $\Delta_0 = -0.15 \pm 0.01$ eV. For the as-cleaved Bi_2Se_3, the work function was measured to be W_F = 5.4 eV, and the initial position of the Dirac point relative to the Fermi level, $E_F - E_D = 0.27$ eV. This yields a value for the electron affinity of neutral MoO_3, $\chi = 5.82 \pm 0.05$ eV.

Last we discuss the use of MoO_3 as both an acceptor dopant and passivation layer for a Bi_2Se_3 thin film, preparing a 15 nm Bi_2Se_3 film by molecular beam epitaxy (MBE) and measuring its electrical transport properties *in situ* in vacuum during deposition of a 100 nm capping layer MoO_3 and continuing to monitor transport on exposure to atmosphere. Figure 4a shows the change in carrier density, $|\Delta n|$ (blue squares), and mobility, μ (green circles), of the Bi_2Se_3 film as a function of MoO_3 coverage. The behavior of the change in carrier density is almost identical to that observed on the as-cleaved Bi_2Se_3 studied with photoemission: a rapid increase in the change in carrier density at low coverage, followed by a saturation after deposition of ~0.1 nm. The overall amount of transferred charge is also very similar at $\sim 10^{13}$ cm^{-2}. The mobility of the film increases to ~430 $cm^2\,V^{-1}\,s^{-1}$ at low MoO_3 coverages then, once the charge transfer process saturates, returns to the initial value of ~390 $cm^2\,V^{-1}\,s^{-1}$, clear evidence that MoO_3 does not degrade the film quality. A further 100 nm of MoO_3 was evaporated as a passivation layer, with negligible further change in carrier density. Following the deposition, the film was exposed to atmosphere. Figure 4b plots the carrier density as a function of exposure time to atmosphere (black circles), with the red dashed line the initial carrier density of the 15 nm film measured after growth but before MoO_3 deposition included as a reference. Over 48 h, the carrier density remains almost unchanged, with only $\sim 5 \times 10^{11}$ cm^{-2} increase in density (consistently seen in other samples) from the initial value upon atmosphere exposure of $n = 1.75 \times 10^{13}$ cm^{-2}. This represents a retention of well over 90% of the initial electron depletion and still $\sim 10^{13}$ cm^{-2} lower than the n-type doping of the as-grown film. This time period is more than long enough for transfer to another cryostat or vacuum system or deposition of additional capping layers. The change in carrier density, $|\Delta n|$, is quantitatively similar to that observed in photoemission for our Bi_2Se_3 crystal surfaces. Our as-grown Bi_2Se_3 thin film has somewhat higher doping and hence higher $E_F - E_D$, and the charge transfer saturation is limited primarily by the doping-induced interface dipole, where $\Delta\Phi \sim \Delta n$; hence we expect similar Δn, in agreement with the observation. This clearly demonstrates the effectiveness of MoO_3 as a passivation layer, protecting the Bi_2Se_3 from reaction with air, which is well-known to increase the n-type doping,[5,26] and preserving the acceptor doping at the Bi_2Se_3−MoO_3 interface. We note that exposure of MoO_3 to air results in a large decrease in the work function from 6.8 to 5.3 eV,[27] which would limit the effectiveness of MoO_3 as an electron acceptor.

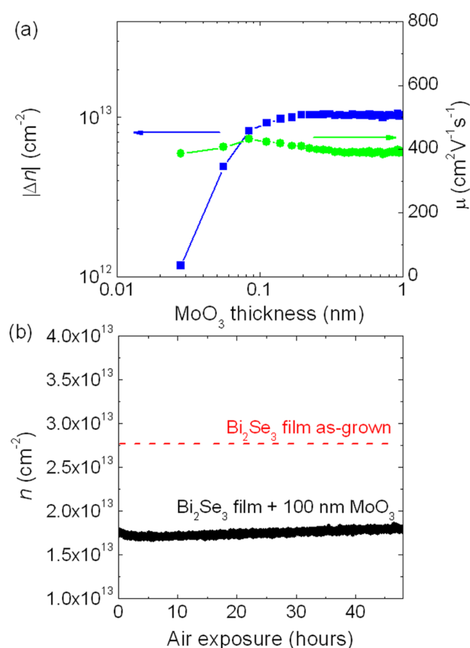

Figure 4. Air-stable acceptor doping of a Bi_2Se_3 film. (a) Change in carrier density $|\Delta n|$ determined from Hall effect measurements plotted as a function of MoO_3 thickness for an MBE-grown Bi_2Se_3 thin film. (b) Electron density of the Bi_2Se_3 film with 100 nm MoO_3 passivation layer plotted as a function of time the sample was exposed to ambient conditions (black circles). The red dashed line is a guide to the eye of the density of the as-grown film.

However, because the charge transfer process saturates well below 1 nm as seen from Figure 4a, the additional MoO_3 layers exposed to air play no role in surface transfer doping and simply act to prevent atmospheric species from reaching and reacting with either the MoO_3 molecules directly involved in charge transfer or the Bi_2Se_3 itself.

CONCLUSION

In conclusion, we identify the molecule MoO_3 as a highly effective acceptor dopant for Bi_2Se_3. High-resolution synchrotron-based photoelectron spectroscopy measurements indicate that MoO_3 doping can bring the surface Fermi energy of Bi_2Se_3 to ~100 meV above the Dirac point, well within the topological regime. We observe two distinct molecular charge components in the Mo 3d core level spectra corresponding to charged and uncharged MoO_3 molecules, allowing a direct measure of the coverage-dependent charge transfer efficiency. A simple model of charge transfer to a discrete molecular level from the Bi_2Se_3 topological surface state accurately describes the coverage dependence of the Fermi energy and interface dipole and gives an initial activation energy for charge transfer of −0.15 eV. Finally, we demonstrate that a thick 100 nm passivation layer of MoO_3 can preserve the acceptor doping from MoO_3 and prevent degradation of Bi_2Se_3 when it is exposed to atmosphere, with the electron density remaining unchanged after 2 days. These findings open up new pathways in Bi_2Se_3 devices, including electronic devices that not only operate in the topological regime but also are stable in air over prolonged periods of time.

EXPERIMENTAL SECTION

Photoelectron Spectroscopy Sample Preparation and Measurement. Low-doped (carrier density ~10^{17} cm^{-3}) bulk Bi_2Se_3 single crystals with bulk resistivity exceeding 2 mΩ cm^{-1} at 300 K were grown by melting high-purity bismuth (6 N) and selenium (5 N) in sealed quartz ampules.[28] Crystals were mounted to a sample holder using conductive epoxy and a cleaving post attached. The samples were then introduced into the ultrahigh vacuum photoemission endstation at the soft X-ray beamline, Australian Synchrotron, where they were subsequently cleaved *in situ* and kept at pressures <10^{-9} mbar during experiments and deposition. F4-TCNQ and MoO_3 (Sigma-Aldrich) were deposited onto the cleaved samples at room temperature using commercial effusion cells (MBE Komponenten GmbH) operating at 135 and 525 °C, respectively, with a quartz crystal microbalance (QCM) used as a guide for the deposition rate. Accurate coverages were determined from the attenuation of the substrate core level spectra. Changes in Fermi level, E_F, in response to surface transfer doping were monitored using both the Bi 5d and Se 3d core level components of Bi_2Se_3 at a photon energy of 100 eV to ensure high surface sensitivity with an overall measurement uncertainty of ±0.02 eV, where the error is defined as one standard deviation. The shift to lower binding energy was the same for both core levels as expected; therefore, we only present and discuss results relating to the Bi 5d core level. In order to determine $E_F - E_D$ from the Bi $5d_{5/2}$ binding energy, we first measured the angle-integrated valence band of a freshly cleaved sample to determine that the Dirac point energy lies 0.27 ± 0.05 eV below the Fermi level (*i.e.*, $E_F - E_D = 0.27 \pm 0.05$ eV), consistent with ARPES results on lightly doped Bi_2Se_3 crystals, where the Fermi level lies just above the bulk conduction band minimum.[23] From this, we determine a fixed separation of the Dirac point to the Bi $5d_{5/2}$ orbital of 24.60 ± 0.05 eV. The ±0.05 eV error represents a systematic uncertainty in determining $E_F - E_D$. The work function was determined from the secondary electron cutoff spectra with an experimental uncertainty of ±0.03 eV. The binding energy scale of all Bi_2Se_3-related spectra is referenced to the Fermi energy (E_F), determined using either the Fermi edge or setting the binding energy of the Au $4f_{7/2}$ core level to be 84.00 eV for a Au reference in electrical contact with the sample. Core level spectra were analyzed using a Shirley background subtraction and then peak-fitted using Voigt functions for each peak component, where the Gaussian and Lorentzian widths of the Bi 5d and Se 3d core level parameters were taken from ref 29. Prior to the experiments, a detailed beam damage study was performed to ensure the molecules were stable under prolonged beam exposure.

Transport Measurements on Bi_2Se_3 Films with 100 nm MoO_3 capping layer. A 15 nm Bi_2Se_3 film was grown by molecular beam epitaxy and its electrical transport properties measured *in situ* in vacuum during deposition of MoO_3 and continually monitored on exposure to atmosphere. The film was grown on a $SrTiO_3$ substrate with pre-existing Ti/Au electrodes in a Hall bar configuration to allow direct measurement of the electrical transport characteristics (resistivity, Hall effect) during film growth and molecular deposition after growth, as described in detail by Hellerstedt *et al.*[30,31] A "two-step" growth method was used:[32] In this instance, 15 nm of Bi_2Se_3 was deposited at 110 °C, and the film was subsequently annealed at 210 °C to improve crystallinity. The 100 nm MoO_3 passivation layer was deposited onto the film at room temperature, with deposition rate determined using a QCM.

Conflict of Interest: The authors declare no competing financial interest.

Acknowledgment. M.S.F. is supported by an ARC Laureate Fellowship, and M.S.F. and J.T.H. are supported by US NSF award DMR-11-05224. Photoemission measurements were performed at the Soft X-ray Beamline of the Australian Synchrotron. This work was performed in part at the Melbourne Centre for Nanofabrication (MCN) in the Victorian Node of the Australian National Fabrication Facility (ANFF). Identification of commercial materials or equipment does not imply recommendation or endorsement by the National Institute of Standards and Technology, nor does it imply that the materials or equipment identified are necessarily the best available for the purpose.

REFERENCES AND NOTES

1. Hasan, M. Z.; Kane, C. L. Colloquium: Topological Insulators. *Rev. Mod. Phys.* **2010**, *82*, 3045–3067.
2. Zhang, H. J.; Liu, C.-X.; Qi, X.-L.; Fang, Z.; Zhang, S.-C. Topological Insulators in Bi_2Se_3, Bi_2Te_3 and Sb_2Te_3 with a Single Dirac Cone on the Surface. *Nat. Phys.* **2009**, *5*, 438–442.
3. Fu, L.; Kane, C. L.; Mele, E. J. Topological Insulators in Three Dimensions. *Phys. Rev. Lett.* **2007**, *98*, 106803.
4. Xia, Y.; Qian, D.; Hsieh, D.; Wray, L.; Pal, A.; Lin, H.; Bansil, A.; Grauer, D.; Hos, Y. S.; Cava, R. J.; *et al.* Observation of a Large-Gap Topological-Insulator Class with a Single Dirac Cone on the Surface. *Nat. Phys.* **2009**, *5*, 398–402.
5. Kong, D.; Cha, J. J.; Lai, K.; Peng, H.; Analytis, J. G.; Meister, S.; Chen, Y.; Zhang, H.-J.; Fisher, I. R.; Shen, Z.-X.; *et al.* Rapid Surface Oxidation as a Source of Surface Degradation Factor for Bi_2Se_3. *ACS Nano* **2011**, *5*, 4698–4703.
6. Hsieh, D.; Xia, Y.; Qian, D.; Wray, L.; Dil, J. H.; Meier, F.; Osterwalder, J.; Patthey, L.; Checkelsky, J. G.; Ong, N. P.; *et al.* A Tunable Topological Insulator in the Spin Helical Dirac Transport Regime. *Nature* **2009**, *460*, 1101–1106.
7. Hor, Y. S.; Richardella, A.; Roushan, P.; Xia, Y.; Checkelsky, J. G.; Yazdani, A.; Hasan, M. Z.; Ong, N. P.; Cava, R. J. p-Type

Bi_2Se_3 for Topological Insulator and Low-Temperature Thermoelectric Applications. *Phys. Rev. B* **2009**, *79*, 195208.
8. Zhang, Y.; Chang, C.-Z.; He, K.; Wang, L.-L.; Chen, X.; Jai, J.-F.; Ma, X.-C.; Xue, Q.-K. Doping Effects of Sb and Pb in Epitaxial Topological Insulator Bi_2Se_3 Thin Films: An *In Situ* Angle-Resolved Photoemission Spectroscopy Study. *Appl. Phys. Lett.* **2010**, *97*, 194102.
9. Hong, S. S.; Cha, J. J.; Kong, D.; Cui, Y. Ultra-low Carrier Concentration and Surface-Dominant Transport in Antimony-Doped Bi_2Se_3 Topological Insulator Nanoribbons. *Nat. Commun.* **2012**, *3*, 757–763.
10. Chen, J.; Qin, H. J.; Yang, F.; Liu, J.; Guan, T.; Qu, F. M.; Zhang, G. H.; Shi, J. R.; Xie, X. C.; Yang, C. L.; *et al.* Gate-Voltage Control of Chemical Potential and Weak Antilocalization in Bi_2Se_3. *Phys. Rev. Lett.* **2010**, *105*, 176602.
11. Kong, D.; Dang, W.; Cha, J. J.; Li, H.; Meister, S.; Peng, H.; Liu, Z.; Cui, Y. Few-Layer Nanoplates of Bi_2Se_3 and Bi_2Te_3 with Highly Tunable Chemical Potential. *Nano Lett.* **2010**, *10*, 2245–2250.
12. Strobel, P.; Riedel, M.; Ristein, J.; Ley, L. Surface Transfer Doping of Diamond. *Nature* **2004**, *430*, 439–441.
13. Greiner, M. T.; Helander, M. G.; Tang, W.-M.; Wang, Z.-B.; Qui, J.; Lu, Z.-H. Universal Energy-Level Alignment of Molecules on Metal Oxides. *Nat. Mater.* **2012**, *11*, 76–81.
14. Tadich, A.; Edmonds, M. T.; Ley, L.; From, F.; Smets, Y.; Mazej, Z.; Riley, J.; Pakes, C. I.; Seyller, Th.; Wanke, M. Tuning the Charge Carriers in Epitaxial Graphene on SiC(0001) from Electron to Hole *via* Molecular Doping with $C_{60}F_{48}$. *Appl. Phys. Lett.* **2013**, *102*, 241601.
15. Smets, Y.; Stark, C. B.; Schmitt, F.; Edmonds, M. T.; Lach, S.; Wright, C. A.; Langley, D. P.; Rietwyk, K. P.; Schenk, A.; Tadich, A.; *et al.* Doping Efficiency and Energy-Level Scheme in $C_{60}F_{48}$-Doped Zinc-Tetraphenylporphyrin Films. *Org. Electron.* **2013**, *14*, 169–174.
16. Kim, D.; Cho, S.; Butch, N. P.; Syers, P.; Kirshenbaum, K.; Adam, S.; Paglione, J.; Fuhrer, M. S. Surface Conduction of Topological Dirac Electrons in Bulk Insulating Bi_2Se_3. *Nat. Phys.* **2012**, *8*, 460–463.
17. Kim, D.; Li, Q.; Syers, P.; Butch, N. P.; Paglione, J.; Das Sarma, S.; Fuhrer, M. S. Intrinsic Electron−Phonon Resistivity of Bi_2Se_3 in the Topological Regime. *Phys. Rev. Lett.* **2012**, *109*, 166801.
18. Kim, D.; Syers, P.; Butch, N. P.; Paglione, J.; Fuhrer, M. S. Coherent Topological Transport on the Surface of Bi_2Se_3. *Nat. Commun.* **2013**, *4*, 2040–2044.
19. Kroger, M.; Hamwi, S.; Meyer, J.; Riedl, T.; Kowalsky, W.; Kahn, A. p-Type Doping of Organic Wide Band Gap Materials by Transition Metal Oxides: A Case-Study on Molybdenum Trioxide. *Org. Electron.* **2009**, *10*, 932–938.
20. Coletti, C.; Riedl, C.; Lee, D. S.; Krauss, B.; Patthey, L.; von Klitzing, K.; Smet, J. H.; Starke, U. Charge Neutrality and Band-Gap Tuning of Epitaxial Graphene on SiC by Molecular Doping. *Phys. Rev. B* **2010**, *81*, 235401.
21. Edmonds, M. T.; Wanke, M.; Tadich, A.; Vulling, H. M.; Rietwyk, K. J.; Sharp, P. L.; Stark, C. B.; Smets, Y.; Schenk, A.; Wu, Q.-H.; *et al.* Surface Transfer Doping of Hydrogen-Terminated Diamond by $C_{60}F_{48}$: Energy Level Scheme and Doping Efficiency. *J. Chem. Phys.* **2012**, *136*, 124701–124709.
22. Kalantar-zadeh, K.; Tang, J.; Wang, M.; Wang, K. L.; Shailos, A.; Galatsis, K.; Kojima, R.; Strong, V.; Lech, A.; Wlodarski, W.; *et al.* Synthesis of Nanometre-Thick MoO_3 Sheets. *Nanoscale* **2010**, *2*, 429–433.
23. Zhu, Z.-H.; Levy, G.; Ludbrook, B.; Veenstra, C. N.; Rosen, J. A.; Comin, R.; Wong, D.; Dosanjh, P.; Ubaldini, A.; Syers, P.; *et al.* Rashba Spin-Splitting Control at the Surface of the Topological Insulator Bi_2Se_3. *Phys. Rev. Lett.* **2011**, *107*, 186405.
24. Kuroda, K.; Arita, M.; Miyamoto, K.; Ye, M.; Jiang, J.; Kimura, A.; Krasovskii, E. E.; Chulkov, E. V.; Iwasawa, H.; Okuda, T.; *et al.* Hexagonally Deformed Fermi Surface of the 3D Topological Insulator Bi_2Se_3. *Phys. Rev. Lett.* **2010**, *105*, 76802.
25. Ley, L.; Smets, Y.; Pakes, C. I.; Ristein, J. Calculating the Universal Energy-Level Alignment of Organic Molecules on Metal Oxides. *Adv. Funct. Mater.* **2013**, *23*, 794–805.
26. Analytis, J. G.; McDonald, R. D.; Riggs, S. C.; Chu, J.-H.; Boebinger, G. S.; Fisher, I. R. Two-Dimensional Surface State in the Quantum Limit of a Topological Insulator. *Nat. Phys.* **2010**, *6*, 960–964.
27. Xie, L.; Wang, X.; Mao, H.; Wang, R.; Ding, M.; Wang, Y.; Özyilmaz, B.; Loh, K. P.; Wee, A. T. S.; Ariando; *et al.* Electrical Measurement of Non-destructively p-Type Doped Graphene Using Molybdenum Trioxide. *Appl. Phys. Lett.* **2011**, *99*, 12112.
28. Butch, N. P.; Kirshenbaum, K.; Syers, P.; Sushkov, A. B.; Jenkins, G. S.; Drew, H. D.; Paglione, J. Strong Surface Scattering in Ultrahigh-Mobility Bi_2Se_3 Topological Insulator Crystals. *Phys. Rev. B* **2010**, *81*, 241301(R).
29. Kuroda, K.; Ye, M.; Schwier, E. F.; Nurmamat, M.; Shirai, K.; Nakatake, M.; Ueda, S.; Miyamoto, K.; Okuda, T.; Namatame, H.; *et al.* Experimental Verification of the Surface Termination in the Topological Insulator $TlBiSe_2$ Using Core-Level Photoelectron Spectroscopy and Scanning Tunneling Microscopy. *Phys. Rev. B* **2013**, *88*, 245308.
30. Hellerstedt, J.; Chen, J. H.; Kim, D.; Cullen, W. G.; Zheng, C. X.; Fuhrer, M. S. *In Situ* Monitoring of Resistivity and Carrier Concentration during Molecular Beam Epitaxy of Topological Insulator Bi_2Se_3. *Proc. SPIE* **2013**, *8923*, 89230–89236.
31. Hellerstedt, J.; Edmonds, M. T.; Chen, J. H.; Cullen, W. G.; Zheng, C. X.; Fuhrer, M. S. Thickness and Growth-Condition Dependence of *In-Situ* Mobility and Carrier Density of Epitaxial Thin-Film Bi_2Se_3. Preprint available at http://arxiv.org/abs/1405.5692.
32. Bansal, N.; Kim, Y. S.; Edrey, E.; Brahlek, M.; Horibe, Y.; Iida, K.; Tanimura, M.; Li, G.-H.; Feng, T.; Lee, H.-D.; *et al.* Epitaxial Growth of Topological Insulator Bi_2Se_3 Film on Si(111) with Atomically Sharp Interface. *Thin Solid Films* **2011**, *520*, 224–229.